Zeolite-Supported Palladium Tetramer and Its Reactivity toward H_2 Molecules: Computational Studies

Jerzy Moc,[†,‡] Djamaladdin G. Musaev,[*,‡] and Keiji Morokuma[*,‡]

Faculty of Chemistry, Wroclaw University, F. Joliot-Curie 14, 50-383 Wroclaw, Poland and Cherry L. Emerson Center for Scientific Computation and Department of Chemistry, Emory University, Atlanta, Georgia 30322

Received: December 3, 2007; Revised Manuscript Received: April 22, 2008

Effects of zeolite support on reactivity of Pd_4 cluster toward dihydrogen molecules were studied at the DFT level using T6 (six-ring) and T24 (sodalite cage) clusters as models of zeolite FAU. It has been found that Pd_4 cluster binds to O-centers of T6 cluster via η^3 and η^2 coordination modes, leading to three different T6/Pd_4 clusters. For the energetically most stable triplet state T6/Pd_4 structures, the energy of interaction between Pd_4 and the constrained T6 ring is calculated to be ca. −5 kcal/mol. Encapsulating Pd_4 in a sodalite cage (T24) with the full relaxation of cluster geometry resulted in the Pd_4−zeolite interaction energy of −7.4 kcal/mol after correcting for basis set superposition error. The H−H bond activation barrier associated with the first H_2 addition to the triplet state T6/Pd_4 clusters ($\Delta E_0/\Delta H$, kcal/mol) varies from (2.2/0.7) to (3.2/2.0) to (4.8/3.5), depending on the path. Comparison of the calculated H_2 addition barriers for the T6-supported and gas-phase Pd_4 indicates that embedding of Pd_4 on zeolite reduces this barrier slightly (by 1.8/2.1 kcal/mol). Interestingly, the characteristic gas phase Pd_4−H_2 active site structural motif has been preserved in the T6-supported transition state structures. The heat of the reaction of the addition of first H_2 to the triplet state T6/Pd_4 ranges from (−17.6/−18.9) to (−21.8/−23.5) for the paths considered. The addition of the second, third and fourth H_2 molecules to the respective first H_2 addition products leads to the dissociative addition product only for the continuation of the single first H_2 addition path.

I. Introduction

Zeolites are crystalline microporous solids used often in chemical industry.[1–3] They possess well-defined structures containing tetrahedral TO_4 building blocks that are connected to each other by sharing O atoms, where T = Si, Al, or other tetrahedrally coordinated atoms. Their features like shape-selective properties, well-defined microporous network[4–6] and good thermal and mechanical stability[7] make them attractive for catalysis.

In the literature, more than hundred distinct zeolite structures have been reported.[1,8] Among them, X- and Y-type zeolites crystallizing in the faujasite (FAU) topology have been the most frequently studied and most commonly utilized in industry as molecular sieves.[9] Structure of the FAU zeolite can be viewed as being made up of sodalite cages (truncated octahedra) connected through the T6 six-rings (T = Si and Al) to form large spherical cavities or supercages of 1.3 nm diameter. Access to the latter is afforded by nonplanar twelve-ring windows with a free aperture of 0.7 nm diameter. After appropriate chemical treatments, zeolites can be employed as acidic, basic and/or redox catalysts, as well as catalyst supports.[4,5] Among numerous reported zeolites, dealuminated or siliceous FAU zeolites have attracted special attention because of their enhanced thermal stability and catalytic properties,[10] especially due to their ability to serve as support for "naked" transition metal (TM) clusters.

Introduction of small "naked" metal clusters into zeolite pores was achieved by CVD (chemical vapor deposition), ship-in-bottle and ion-exchange methods or decarbonylation of carbonyl clusters.[4] The resulted metal clusters in zeolites were investigated mainly from the perspective of formation of uniform active sites for catalytic reactions.[4b] During the past decade or so, numerous experimental studies on the incorporation of small palladium clusters inside pores of FAU zeolites have been reported.[11,12] The transmission electron microscopy (TEM) and extended X-ray absorption fine structure (EXAFS) techniques have provided clear evidence on the presence of small Pd_n clusters (n = 1−4,6,13) inside sodalite cages and supercages of FAU zeolites.[11,12] Pure silica-supported palladium clusters were also prepared.[13]

In the preceding studies we have investigated structures and sequential H_2 addition to the "naked" (gas-phase) Pd_n clusters (n = 2−5).[14] In the present work, we focus on examining the effects of the FAU zeolite support on the course of this hydrogenation process. With the purely siliceous faujasite chosen here as the zeolite support and lacking framework Al atoms and extra framework charge-balancing cations, the atoms of TM cluster represent the only active sites capable of H_2 molecular/dissociative adsorption. The effects of purely siliceous FAU zeolite framework on the Pd_n hydrogenation were evaluated for palladium tetramer Pd_4.

II. Zeolite Models and Computational Methods

The unit cell of FAU zeolite contains several hundred atoms,[8,10,15] which makes its computational studies challenging and requiring special approaches. The most popular approach of modeling zeolite is a cluster approach.[16] The majority of calculations performed in the present paper adopts the cluster T6 represented by the single six-ring (six T = Si atoms and six O atoms),[10] where the T's dangling bonds were capped with

* Corresponding authors.
† Wroclaw University.
‡ Emory University.

10.1021/jp711403x CCC: $40.75
Published on Web 06/11/2008

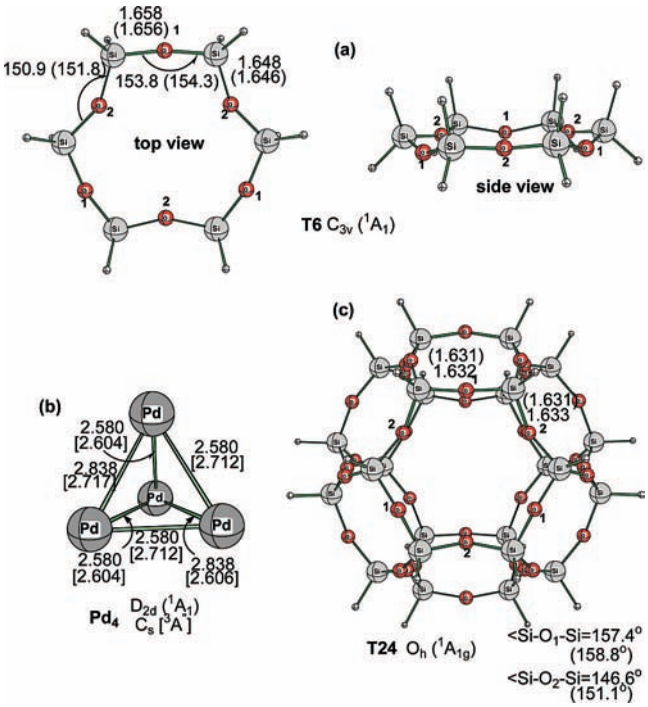

Figure 1. Important geometry parameters of the T6 (six-ring, $Si_6O_6H_{12}$) and T24 (sodalite cage, $Si_{24}O_{36}H_{24}$) models of zeolite, as well as free Pd_4 cluster (taken from ref 14b, values given without and with brackets are for singlet and triplet states, respectively). Distances are in angstroms, and angles are in deg, calculated at B3LYP/HWDZP and MP2/6-311G(d) (in parentheses) level of theory. The calculated B3LYP/HWDZP NPA charges of the O_1, O_2 and Si atoms of T6 cluster are −1.31e, −1.32e and +1.83e, respectively.

hydrogen atoms, $Si_6O_6H_{12}$ (Figure 1a)[16] as a model of FAU zeolite. The T6 ring constitutes a part of the wall of sodalite cage that faces toward the supercage of FAU zeolite.[8,15] The model cluster with the same size (but with three T = Si and three T = Al atoms) was previously found to be appropriate for studying interaction of Ir_4 with FAU zeolite by Rösch et al.[17] To study the effects of encapsulating Pd_4 within the zeolite cage, the T24 cluster consisting of the entire sodalite cage, $Si_{24}O_{36}H_{24}$, was also used as a model of FAU zeolite, where the hydrogen atoms were applied to saturate the T's dangling bonds.

In the present study, as in the case of free (unsupported) Pd_4,[14b] the T6 and T24 supported Pd_4 cluster, designated as **T6/Pd$_4$** and **T24/Pd$_4$**, respectively, and the reaction of the former cluster with H_2 molecules were calculated at the DFT (B3LYP) level.[18] During the geometry optimization of T6 and **T6/Pd$_4$** clusters, the location of capping hydrogens were fixed at the starting positions. This geometry constraint was imposed to prevent artificial interactions between the hydrogens and Pd_4 that occurred upon relaxation of geometry of the entire cluster (leading to nonzeolitic type structures). The optimization of structures was followed by normal-mode frequency analysis (under the imposed geometry constraints). The effective core potential (ECP) of Hay and Wadt (HW)[19] on the Pd and Si atoms was used with the valence double-ζ (VDZ) quality basis set on Pd and the polarized VDZ basis set on Si. For O and H atoms, the polarized all-electron double-ζ quality basis sets were used.[20] This computational level, denoted as B3LYP/HWDZP, was previously used to study the $Pd_4 + nH_2$ reactions.[14b] The use of Hay and Wadt ECP for Si, as shown recently, provides a reliable description of the silicon surfaces.[21] In addition, for the T6 and T24 clusters, we compared the B3LYP/HWDZP structures with the MP2/6-311G(d)[22,23] ones (see below). For better energetics, we performed single point calculations using ECP of Dolg and co-workers on Pd and valence triple-ζ quality basis sets for Pd and H[14b,24] along with the 6-311G(2d) basis set for Si and O[23] (B3LYP/TZP level). This is the same level as we used for the gas phase ("naked")[14b] cluster and allows a meaningful comparison of the final energetics with the zeolite-supported clusters.

The **Pdn_x_yi_z** notation introduced before[14b,c] for a systematic description of the palladium/hydrogen clusters is being used below for consistency. Here, "**n**" is a number of TM atoms; "**x**" shows which H_2 molecule (**1**st, **2**nd, etc.) enters the reaction; "**y**" describes the nature of the species, where **y** = **a**, **a′**, ... corresponds to dihydrogen complex, **y** =**b**, **b′**, ... indicates the H−H activation transition state (TS), **y** = **c**, **c′**, ... denotes the H−H activated product. Here **i** corresponds to the Path(i) (where **i** = 1, 2 and 3, see below); and "**z**" shows the position of the H ligands in the activated system. Within the activated system, the H ligand can (1) occupy the single (terminal) Pd atom, or (2) bridge the edge of the Pd−Pd bond, or (3) cap the Pd−Pd−Pd face. These three binding sites are denoted "**t**", "**e**", and "**f**", respectively. Furthermore, because the clusters calculated here have an even number of H ligands, "**z**" is going to have an even number of components. For instance, in case of two H ligands, (**e,e**) indicates that they bridge two different Pd−Pd edges sharing a Pd atom, whereas (**e,e′**) shows that the two H ligands bridge two different Pd−Pd edges not sharing any Pd atom. Similarly, (**e,f**) indicates that the first H ligand bridges a Pd−Pd edge and the second one caps a Pd−Pd−Pd face, which share a Pd atom or a Pd−Pd edge, whereas (**e,f′**) relates to the situation when the bridging and cap sites do not share a Pd atom or a Pd−Pd edge. Also, (**f,f**) shows both H ligands in cap sites that share a Pd−Pd edge, and so on. Note that for four, six, ... H-ligands, "**z**" has four, six, ... components, respectively.

The adsorption energy of Pd_4 on the T6 (or T24) model cluster is calculated as follows:

$$\Delta E = E[\text{T6(T24)/Pd}_4] - \{E[\text{Pd}_4,\text{ground-state}] + E[\text{T6(T24)}]\}$$

The adsorption energy of the H_2 molecule on the T6 zeolite-supported Pd_4 is defined as

$$\Delta E = E[\text{T6/Pd}_4(\text{H}_2)] - \{E[\text{T6/Pd}_4] + E(\text{H}_2)\} \quad \text{(molecular)}$$

$$\Delta E = E[\text{T6/Pd}_4(\text{H})_2] - \{E[\text{T6/Pd}_4] + E(\text{H}_2)\} \quad \text{(dissociative)}$$

Thus, consistent with our earlier calculations,[14b] a negative value of ΔE indicates an exothermic process. The calculations were performed using Gaussian 03.[25]

III. Results and Discussion

A. T6 and T6/Pd$_4$. At first we discuss the binding of Pd_4 to the T6 ring. The B3LYP/HWDZP and MP2/6-311G(d) calculated C_{3v} structure of the T6, shown in Figure 1a, reveals a good agreement between the ECP and all-electron (in parentheses) results. In this structure, there are six bridging oxygens with alternating bending in and out positions and denoted throughout as O_2 and O_1, respectively. These two kinds of oxygens provide, independently, the 3-fold adsorption/coordination sites for Pd_4. Previously, we[14b] and other authors[26] have established the triplet $^3A''$ state in C_s symmetry to be the ground electronic state of

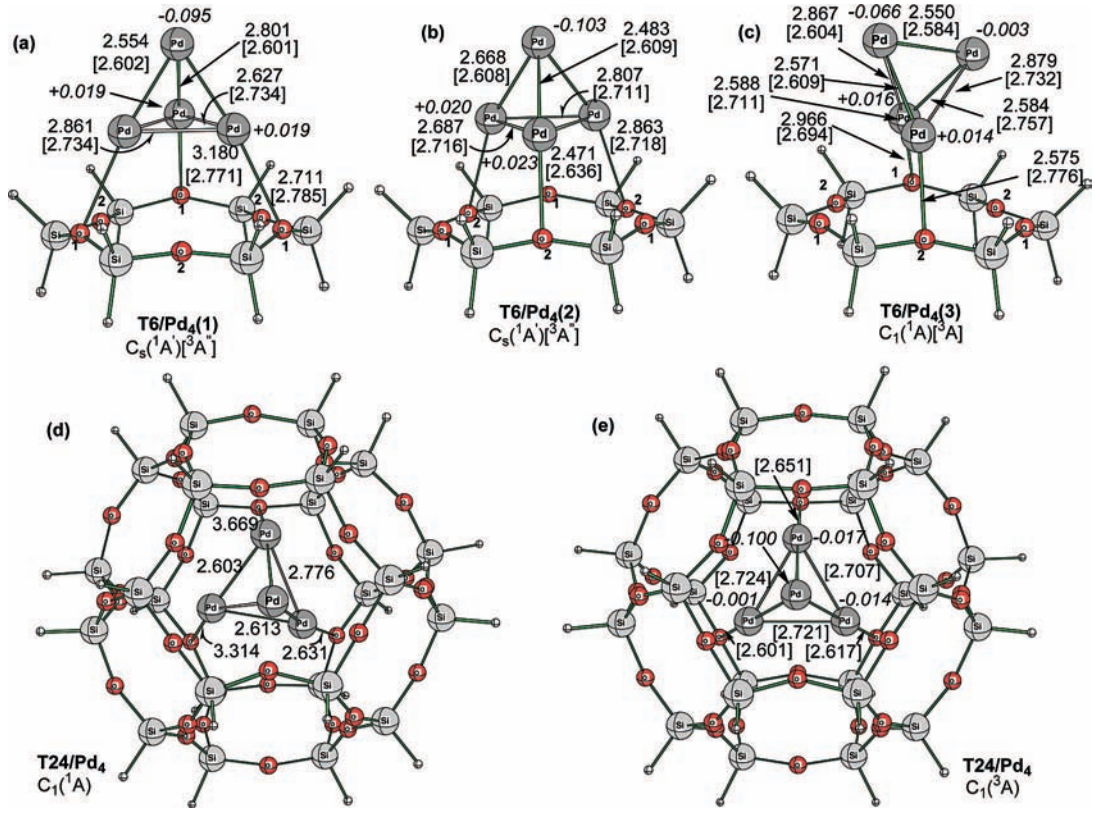

Figure 2. Singlet and triplet state structures (distances in Å, in brackets for triplet) of the T6- and T24-supported Pd_4 clusters: (a) Pd atoms of Pd_4 interact with the three O_1 oxygens of T6, **T6/Pd$_4$(1)**; (b) Pd atoms of Pd_4 interact with the three O_2 oxygens of T6, **T6/Pd$_4$(2)**; (c) Pd_4 cluster interacts via its Pd−Pd edge with T6 ring, **T6/Pd$_4$(3)**; (d) singlet and (e) triplet Pd_4 cluster encapsulated within the T24 cage (**T24/Pd$_4$**). The calculated B3LYP/HWDZP NPA charges are given in italic for the lower energy triplet states of T6/Pd_4 and T24/Pd_4 clusters.

the isolated Pd_4 with the Pd−Pd distances of 2.60−2.72 Å. Its lowest singlet state (D_{2d},$^1A_1$) lies 16.8 kcal/mol higher in energy and has the Pd−Pd distances of 2.58−2.84 Å (Figure 1b).

Pd_4 cluster can interact with the T6 support by its: (i) Pd−Pd−Pd base; (ii) Pd−Pd edge; and (iii) Pd apex. For the binding mode (i), we have found two local-minima (for each spin state) for T6/Pd_4 arising from the interaction of Pd_4 base predominantly with the three O_1, **T6/Pd$_4$(1)**, and O_2, **T6/Pd$_4$(2)**, sites, respectively (see Figure 2). The C_s symmetry was assumed for the two clusters.[27] For the binding mode (ii), we have found one minimum (for each spin state), **T6/Pd$_4$(3)**. The binding mode (iii) appeared to be less favorable[28] (the corresponding T6/Pd_4 cluster is included in Supporting Information). Like the isolated Pd_4,[14b] the zeolite-supported Pd_4 cluster has a triplet ground state (Table 1). As seen in Figure 2, the triplet **T6/Pd$_4$(1)**(^{3}A″) exhibits three shorter Pd−O_1 bonds of 2.77−2.79 Å (with longer Pd−O_2 distances of 3.45−3.47 Å). Similarly, **T6/Pd$_4$(2)**(^{3}A″) features three shorter Pd−O_2 distances of 2.64−2.72 Å (with longer Pd−O_1 distances of 3.51−3.55 Å).[29a] In **T6/Pd$_4$(3)**(^{3}A), the calculated Pd−O_1 and Pd−O_2 distances are 2.69 and 2.78 Å. The calculated Pd−O distances for all these structures are consistent with the metal−oxygen separations of 2.74−2.76 Å inferred from the EXAFS analysis of the small Pd_n clusters (n = 2−4) supported by the NaX FAU zeolite.[11a,29b]

The calculated Pd−Pd bond lengths of the **T6/Pd$_4$(1)**(^{3}A″), **T6/Pd$_4$(2)**(^{3}A″) and **T6/Pd$_4$(3)**(^{3}A) clusters are 2.60−2.73, 2.61−2.72 and 2.58−2.76 Å, respectively, which are very close to those in the isolated Pd_4(^{3}A″) cluster. These geometrical parameters along with the preserved tetrahedral-like shape of the isolated Pd_4 in T6/Pd_4 indicate a weak Pd_4−T6 interaction. Indeed, the calculated $\Delta E_0/\Delta H$ values for the Pd_4−T6 interaction are −5.3/−4.5, −4.9/−4.0 and −4.9/−4.0 kcal/mol, for **T6/Pd$_4$(1)**(^{3}A″), **T6/Pd$_4$(2)**(^{3}A″) and **T6/Pd$_4$(3)**(^{3}A) clusters, respectively (throughout this paper, we use both the zero-point energy (ZPE) corrected relative energies (ΔE_0) and enthalpies at 298.15 K (ΔH), presented in the $\Delta E_0/\Delta H$ manner (Table 1)). This conclusion is also supported by the calculated spin states of the supported and free Pd_4: in both cases the system has the triplet ground-state and its singlet state lie higher by 17.7/17.8, 19.3/18.2, 16.4/16.4, and 16.8/16.8 kcal/mol for the **T6/Pd$_4$(1)**, **T6/Pd$_4$(2)**, **T6/Pd$_4$(3)**, and Pd_4[14b] clusters, respectively (Table 1).

TABLE 1: Calculated Adsorption Energies (in kcal/mol) of Pd_4 on the T6 and T24 Clusters, at the B3LYP/TZP// B3LYP/HWDZP Level

T6/Pd_4 supported cluster[a]	ΔE_0[b]	ΔE_0[c]	ΔH[d]
T6/Pd$_4$(1)(^{3}A″)	−5.4	−5.3	−4.5
T6/Pd$_4$(1)(^{1}A′)	12.4	12.4	13.3
T6/Pd$_4$(2)(^{3}A″)	−4.9	−4.9	−4.0
T6/Pd$_4$(2)(^{1}A′)	14.5	14.4	14.2
T6/Pd$_4$(3)(^{3}A)	−5.0	−4.9	−4.0
T6/Pd$_4$(3)(^{1}A)	11.4	11.5	12.4
T24/Pd$_4$(^{3}A)	−20.3(−7.4)[e]		
T24/Pd$_4$(^{1}A)	−1.3(11.8)[e]		

[a] See Figure 1 for the definition of T6/Pd_4 clusters. [b] $\Delta E = E$(T6/Pd_4) − [E(Pd_4,^{3}A″) + E(T6)]; for T24/Pd_4, $\Delta E = E$(T24/Pd_4) − [E(Pd_4,^{3}A″) + E(T24)]. [c] $\Delta E_0 = \Delta E$ + ΔZPE, zero-point energy corrections were calculated at the B3LYP/HWDZP level. [d] ΔH, enthalpies were calculated at the 1 atm and 298.15 K at the B3LYP/TZP//B3LYP/HWDZP level. [e] Values in parentheses have been BSSE corrected (see text).

Our results for the T6 zeolite-supported Pd_4 clusters are consistent with the recent DFT study by Rösch et al. of the

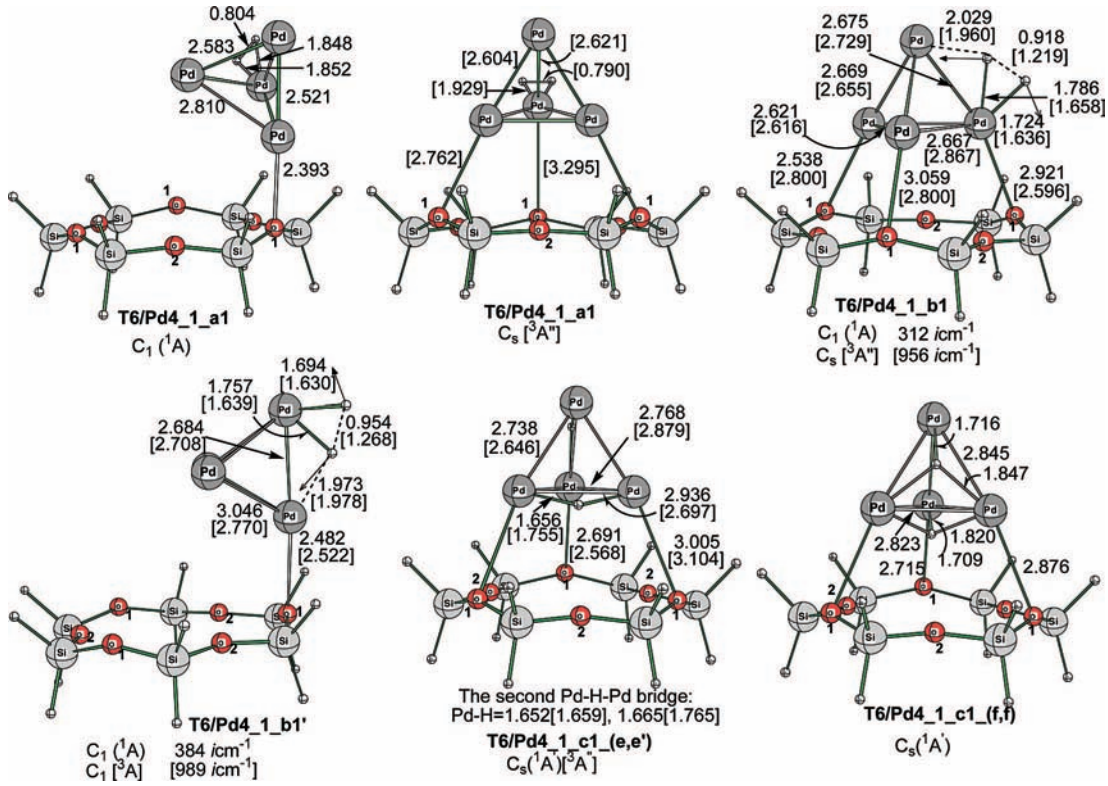

Figure 3. Important geometry parameters (distances in Å, in brackets for triplet) of the intermediates, transition states (with imaginary frequency and reaction coordinate vectors) and products of the singlet and triplet state reaction (Path 1): **T6/Pd$_4$(1)** + H_2.

supported transition metal M_6 clusters of groups 8−10.[30] Among the 12 hexamers examined by these authors, the Pd_6 adsorption energy on the constrained six-ring model FAU zeolite cluster (three T = Si and three T = Al atoms) was found to be the lowest (−12.9 kcal/mol), with the retained triplet state and gas phase shape of the isolated Pd_6. Within Group 10, the largest binding effect to the zeolite was predicted for Pt_6.[30]

The relatively weak Pd_4−T6 interaction is also reflected in modest polarization and charge-transfer between Pd_4 and T6, as shown in the B3LYP/HWDZP NPA[31] charges (in italic) in Figure 2. For **T6/Pd$_4$(1)**(^{3}A″) and **T6/Pd$_4$(2)**(^{3}A″), the Pd atoms directly bound to the O_1 and O_2 oxygens bear +0.019, +0.019 and +0.019 e, and +0.020, +0.020 and +0.023 e positive charges, respectively. By contrast, the on-top Pd atoms of these clusters show the slightly negative charge of ca. −0.10 e. In case of **T6/Pd$_4$(3)**(^{3}A), the Pd atoms coordinated to the O_1 and O_2 oxygen sites are again positively charged, by +0.016 and +0.014 e, whereas the two "upper layer" Pd centers are negatively charged by −0.003 and −0.066 e, respectively. Thus, the NPA analysis suggests the existence of two kinds of Pd centers in T6/Pd_4 clusters; those directly coordinated to T6 with small cationic character and "upper layer" Pd atoms showing small anionic character. Consequently, the Pd centers of each kind might show somewhat different reactivity toward H_2. A small total charge transfer occurs from T6 to Pd_4: 0.038, 0.040 and 0.071 e for **T6/Pd$_4$(1)**, **T6/Pd$_4$(2)** and **T6/Pd$_4$(3)**, respectively.

B. T24 and T24/Pd$_4$. The T24 cluster (twenty four T = Si atoms and twenty four O atoms) represents the sodalite cage of FAU zeolite (Figure 1c). At the B3LYP/HWDZP level, it exhibits Si−O_1 and Si−O_2 bond lengths 1.632−1.633 Å, shorter by 0.015−0.026 Å compared to those of T6 cluster. The calculated Si−O_1−Si and Si−O_2−Si bond angles of T24 cluster, 157.4 and 146.6°, respectively, are within 4° of the T6 angles. Additional geometry optimization of the T24 at the MP2/6-311G(d) level (1344 basis functions) essentially does not change the Si−O distances, the largest deviation between the ECP and all-electron (in parentheses) results of 4.5° is seen for the Si−O_2−Si angle. To assess the binding effects of Pd_4 encapsulated in the sodalite cage, the Pd_4 adsorption via its Pd−Pd−Pd base on one of T6 rings inside the cage of T24 cluster has been examined. Geometry of this cluster was fully optimized without symmetry constraints for both singlet and triplet electronic states. The resulting structures of **T24/Pd$_4$** are given in Figure 2. The lower energy triplet state structure **T24/Pd$_4$**(^{3}A) features the preserved (from the **T6/Pd$_4$(1)**(^{3}A″) cluster) η^3 Pd−O_1 coordination mode, with three Pd−O_1 bonds of 2.60−2.65 Å, which are shortened noticeably by 0.13−0.17 Å relative to those in **T6/Pd$_4$(1)**(^{3}A″). In the singlet electronic state, the cage confinement leads to the more asymmetric (nearly C_{3v}) Pd_4−T24 binding realized primarily by the Pd−O_1 contact at 2.63 Å; this distance is smaller by 0.08 Å than that of the T6 model.

On the other hand, as seen before for the T6-supported Pd_4 cluster, the calculated Pd−Pd bond lengths in **T24/Pd$_4$**(^{3}A) of 2.61−2.72 Å are not substantially changed compared to those in the isolated Pd_4(^{3}A″). Thus, no significant distortion or disintegration of Pd_4 entrapped in the cage takes place. This is consistent with the calculated interaction energy (ΔE) of Pd_4 inside the sodalite cage with respect to the gas phase Pd_4(^{3}A″) separated from the cage (Table 1). Although the initially computed interaction energy in **T24/Pd$_4$** of −20.3 kcal/mol (triplet) and –1.3 kcal/mol (singlet) would indicate significantly stronger interaction than in **T6/Pd$_4$**, after correcting for a basis set superposition error (BSSE)[32] ΔE of −7.4 kcal/mol (triplet) and 11.8 kcal/mol (singlet) (Table 1, in parentheses) becomes comparable to that obtained using the constrained T6 model and discussed above. The B3LYP/HWDZP NPA charges for **T24/Pd$_4$**(^{3}A) (Figure 2e, in italic) are consistent with those obtained for **T6/Pd$_4$(1)**(^{3}A″) in showing the modest polarization and charge transfer between Pd_4 and zeolite. In particular, the two zeolite models find the negatively charged on-top Pd atom,

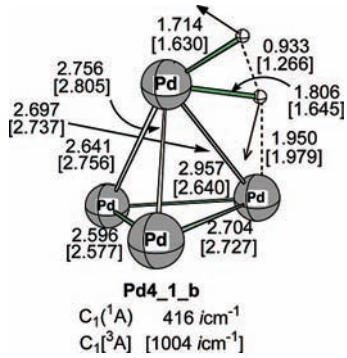

Figure 4. Important geometry parameters (distances in Å, in brackets for triplet) of the gas phase transition states (**Pd4_1_b**, from ref 14b) of the reaction $Pd_4 + H_2$.

by ca. 0.10 e. For **T24/Pd$_4$**(^{3}A), the Pd atoms directly coordinated to the oxygens bear slightly negative charge of −0.001, −0.014 and −0.017 e.

C. First H_2 on T6/Pd$_4$. Next we discuss adsorption/activation of the first H_2 molecule on **T6/Pd$_4$(1)**, **T6/Pd$_4$(2)** and **T6/Pd$_4$(3)** clusters. The corresponding reaction paths are called Path(1), Path(2) and Path(3), respectively. We have chosen the smaller T6 zeolite cluster for these extensive and computationally demanding studies. In these studies, we are particularly interested in the influence of zeolite support on the structures and energy of the H_2 coordination and activation on Pd_4. Let us recall that the H_2 addition to unsupported ground-state triplet Pd_4 proceeds via formation of a triplet reactant complex $Pd_4(H_2)$, followed by the H−H dissociation through a triplet transition state and formation of a dihydride product $Pd_4(H)_2$.[14b] Because the dihydride product has a singlet ground state, the system is expected to make crossing from triplet to singlet somewhere between the transition state and the final singlet product. The two most stable isomers of the final $Pd_4(H)_2$ product were singlet state structures of (**e,e′**) and (**f,f**) type, i.e., with the two H's bridging the not-shared Pd−Pd edges and Pd−Pd−Pd faces, respectively.[14b] We have indicated above that the Pd_4−T6 interaction is relatively weak. Thus, it is reasonable to assume that the gas-phase structures of dihydrogen complexes, H−H activation transition states and dihydride products of the Pd_4/H_2 system[14b] will be relevant to the study of the T6/Pd_4/H_2 system. No initial symmetry was imposed during geometry optimization of the hydrogenated T6/Pd_4 clusters. Below, we discuss Path 1, 2 and 3 in detail.

Path(1). As seen in Figure 3, reaction of **T6/Pd$_4$(1)** with H_2 molecule involves the same elementary steps encountered for the analogous gas phase reaction $Pd_4 + H_2$. It can proceed via two distinct ways: via the attack of H_2 molecule on the *basal* and *apical* Pd centers. We first examine the *basal* attack of H_2, i.e. toward the Pd atom bound to the T6 fragment (see Figure 3). The resulting singlet state complex **T6/Pd4_1_a1**(^{1}A) displays a shortest Pd−O_1 distance of 2.39 Å. However, the other two Pd−O_1 bonds (including the one with the Pd involved in the H_2 adsorption) that existed in the singlet state reference **T6/Pd$_4$(1)** cluster are lost. In the case of the more stable triplet state complex **T6/Pd4_1_a1**(^{3}A″) all three Pd−O_1 contacts exist with the 2.76, 2.76 and 3.29 Å distances. It is seen, however, that the Pd−O_1 distance engaging Pd atom that interacts with H_2 is significantly elongated. These results clearly show that

TABLE 2: Calculated Relative Energies (Relative to the Corresponding Reactants, in kcal/mol) of the Intermediates, Transition States and Products of the Reactions: T6/Pd$_4$(i) + H_2, where i = 1, 2 and 3 at the B3LYP/TZP//B3LYP/HWDZP Level[a]

supported cluster		ΔE		ΔE_0[b]		ΔH[c]	
Path(1)							
T6/Pd$_4$(^{3}A″) + H_2	**T6/Pd$_4$(1)**(^{3}A″) + H_2	0.0	*0.0*	0.0	*0.0*	0.0	*0.0*
T6/Pd$_4$(^{1}A′) + H_2	**T6/Pd$_4$(1)**(^{1}A′) + H_2	17.8	*16.8*	17.7	*16.8*	17.8	*16.8*
T6/Pd$_4$(H_2)(^{3}A″)	**T6/Pd4_1_a1**(^{3}A″)	−7.6	*−8.8*	−5.9	*−7.0*	−6.7	*−7.7*
basal TS (^{3}A″)	**T6/Pd4_1_b1**(^{3}A″)	3.6	*4.4*	3.2	*4.0*	2.0	*2.8*
apical TS (^{3}A)	**T6/Pd4_1_b1′**(^{3}A)	5.2	*4.4*	4.8	*4.0*	3.7	*2.8*
T6/Pd$_4$(H)$_2$(^{3}A″)	**T6/Pd4_1_c1_(e,e′)**(^{3}A″)	−7.5	*−8.3*	−6.8	*−7.6*	−8.1	*−8.9*
T6/Pd$_4$(H_2) (^{1}A)	**T6/Pd4_1_a1**(^{1}A)	4.8	*6.9*	7.1	*9.0*	6.0	*8.0*
basal TS (^{1}A)	**T6/Pd4_1_b1**(^{1}A)	13.7	*13.3*	14.2	*13.8*	12.8	*12.2*
apical TS (^{1}A)	**T6/Pd4_1_b1′**(^{1}A)	12.8	*13.3*	13.1	*13.8*	11.6	*12.2*
T6/Pd$_4$(H)$_2$ (^{1}A′)	**T6/Pd4_1_c1_(e,e′)**(^{1}A′)	−19.5	*−20.9*	−17.6	*−19.0*	−18.9	*−20.3*
T6/Pd$_4$(H)$_2$ (^{1}A′)	**T6/Pd4_1_c1_(f,f)**(^{1}A′)	−18.1	*−19.3*	−17.0	*−18.3*	−18.6	*−20.0*
Path(2)							
T6/Pd$_4$(^{3}A″) + H_2	**T6/Pd$_4$(2)**(^{3}A″) + H_2	0.0	*0.0*	0.0	*0.0*	0.0	*0.0*
T6/Pd$_4$(^{1}A′) + H_2	**T6/Pd$_4$(2)**(^{1}A′) + H_2	19.4	*16.8*	19.3	*16.8*	18.2	*16.8*
T6/Pd$_4$(H_2)(^{3}A″)	**T6/Pd4_1_a2**(^{3}A″)	−8.1	*−8.8*	−6.3	*−7.0*	−7.3	*−7.7*
TS (^{3}A″)	**T6/Pd4_1_b2**(^{3}A″)	2.1	*4.4*	2.2	*4.0*	0.7	*2.8*
T6/Pd$_4$(H)$_2$(^{3}A)	**T6/Pd4_1_c2_(e,f)**(^{3}A)	−7.5	*−5.2*	−7.0	*−5.1*	- 8.5	*−6.4*
T6/Pd$_4$(H_2)(^{1}A)	**T6/Pd4_1_a2**(^{1}A)	6.2	*6.9*	8.4	*9.0*	7.3	*8.0*
TS (^{1}A)	**T6/Pd4_1_b2**(^{1}A)	9.5	*13.3*	10.4	*13.8*	8.7	*12.2*
T6/Pd$_4$(H)$_2$ (^{1}A′)	**T6/Pd4_1_c2_(e,e′)**(^{1}A′)	−19.4	*−20.9*	−17.7	*−19.0*	−19.5	*−20.3*
T6/Pd$_4$(H)$_2$ (^{1}A′)	**T6/Pd4_1_c2_(f,f)**(^{1}A′)	−20.5	*−19.3*	−19.2	*−18.3*	−21.0	*−20.0*
Path(3)							
T6/Pd$_4$(^{3}A″) + H_2	**T6/Pd$_4$(3)**(^{3}A″) + H_2	0.0	*0.0*	0.0	*0.0*	0.0	*0.0*
T6/Pd$_4$(^{1}A′) + H_2	**T6/Pd$_4$(3)**(^{1}A′) + H_2	16.4	*16.8*	16.4	*16.8*	16.4	*16.8*
T6/Pd$_4$(H_2)(^{3}A)	**T6/Pd4_1_a3**(^{3}A)	−7.9	*−8.8*	−6.2	*−7.0*	−7.0	*−7.7*
TS (^{3}A)	**T6/Pd4_1_b3**(^{3}A)	5.4	*4.4*	4.8	*4.0*	3.5	*2.8*
T6/Pd$_4$(H)$_2$(^{3}A)	**T6/Pd4_1_c3_(e,e′)**(^{3}A)	−8.1	*−8.3*	−6.3	*−7.6*	−7.3	*−8.9*
T6/Pd$_4$(H_2)(^{1}A)	**T6/Pd4_1_a3**(^{1}A)	6.2	*6.9*	8.3	*9.0*	7.2	*8.0*
TS (^{1}A)	**T6/Pd4_1_b3**(^{1}A)	12.8	*13.3*	13.2	*13.8*	11.6	*12.2*
T6/Pd$_4$(H)$_2$ (^{1}A′)	**T6/Pd4_1_c3_(f,f)**(^{1}A′)	−22.8	*−19.3*	−21.8	*−18.3*	−23.5	*−20.0*

[a] Values given in italics are for the gas-phase reaction: $Pd_4 + H_2$, taken from the ref 14b. See Figure 2 for the definition of the T6/Pd_4 clusters. [b] $\Delta E_0 = \Delta E + \Delta$ZPE, zero-point energy corrections were calculated at the B3LYP/HWDZP level. [c] ΔH, enthalpies were calculated at the 1 atm and 298.15 K at the B3LYP/TZP//B3LYP/HWDZP level.

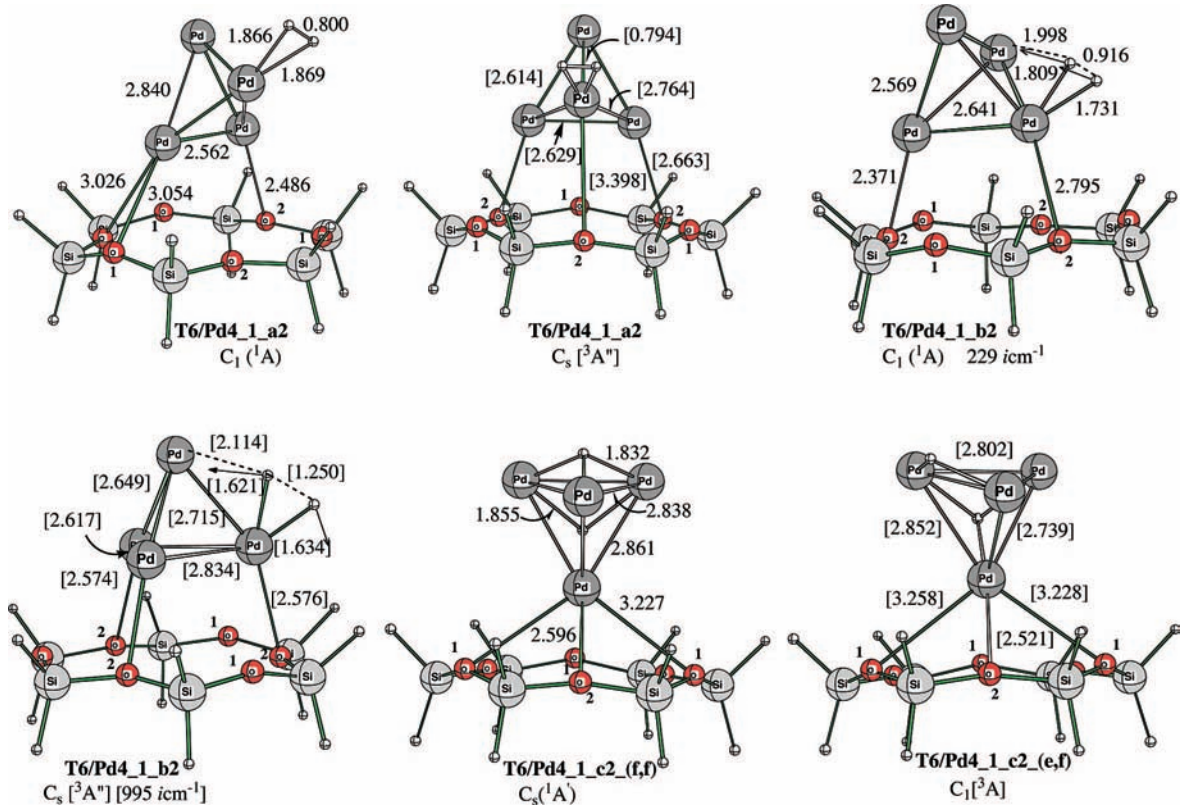

Figure 5. Important geometry parameters (distances in Å, in brackets for triplet) of the intermediates, transition states (with imaginary frequency and reaction coordinate vectors) and products of the singlet and triplet state reaction (Path 2): **T6/Pd$_4$(2)** + H_2.

due to the accompanying charge reorganization, the Pd−O_1 interaction involving the Pd atom that serves as H_2 adsorption site is either essentially lost (singlet state structure) or substantially weakened (triplet state structure).

Bearing in mind that the Pd_4-zeolite interaction leads to neither spin quenching nor the major transition metal cluster geometry changes, one would anticipate similar structural parameters for the H−H activation TS in gas-phase and on zeolite support. This assumption is corroborated by the actual calculations. The located singlet and triplet state TSs, **T6/Pd4_1_b1**, for the H−H activation on the *basal* position of T6−Pd_4 cluster are given in Figure 3. For comparison, the corresponding gas-phase transition states[14b] are shown in Figure 4. As seen from Figures 3 and 4, in the zeolite-supported singlet state TS, **T6/Pd4_1_b1**, one can easily notice the conserved feature of the corresponding gas-phase transition state: the breaking H−H bond positioned parallel (or nearly so) to the Pd−Pd edge. As in the singlet state reference cluster **T6/Pd$_4$(1)**, this TS binds to the support via three Pd−O_1 contacts, however, with the significantly changed distances relative to those in the reference cluster (cf. Figures 2 and 3). Interestingly, the breaking H−H distance, of 0.918 Å, in the singlet state **T6/Pd4_1_b1** is decreased by 0.015 Å compared to 0.933 Å in the gas-phase TS **Pd4_1_b**. Thus, the T6-supported singlet state H−H activation TS is somewhat "earlier" transition state than its gas phase analog. A similar feature is also visible for the lower energy triplet state TS **T6/Pd4_1_b1**(^{3}A″); the breaking H−H bond of 1.219 Å is situated again parallel to the Pd−Pd edge and shorter by 0.047 Å relative to that in unsupported TS of 1.266 Å. Another important structural feature of the T6-supported triplet state TS **T6/Pd4_1_b1**(^{3}A″) is the existence of three Pd−O_1 contacts with the distances of 2.60, 2.80 and 2.80 Å.

We have also calculated the transition state **T6/Pd4_1_b1′** (at its singlet and triplet electronic states) corresponding to the *apical* attack of H_2 molecule (see Figure 3). In this structure, the Pd atom that is located on the top position and not being in direct contact with T6-support serves as the H_2 activation center (The *apical* H_2 complex **T6/Pd4_1_a1′** for this higher energy Path(1), see below, is included in the Supporting Information). As seen in Figure 3, the located *apical* transition states are different from their *basal* analogs. Indeed, at the *apical* TS, **T6/Pd4_1_b1′**, Pd_4 cluster is situated much more asymmetrically over the six-centered-ring of T6, and interacts with it predominantly through the single Pd−O_1 contact; the calculated Pd−O_1 distance is 2.522 and 2.482 Å for the triplet and singlet state structures, respectively. Comparison of the structure of **T6/Pd4_1_b1′** with the transition state for unsupported Pd_4, **Pd4_1_b** (see Figure 4), indicates that the *apical* TS preserves all the features of unsupported-Pd_4−H_2 active site. However, the *apical* T6-supported TS's are somewhat late transition states in terms of the breaking H−H distance (with respect to **Pd4_1_b**(^{1}A, ^{3}A)), which is 0.954 and 1.268 Å for the singlet and triplet state TSs, respectively.

Paralleling the gas-phase behavior,[14b] the energetically most favorable products of the reaction **T6/Pd$_4$(1)** + H_2 (i.e., Path(1)) are singlet state **T6/Pd4_1_c1_(e,e′)** and **T6/Pd4_1_c1_(f,f)** clusters. Structure **T6/Pd4_1_c1_(e,e′)** contains two H-atoms on two unshared Pd−Pd edges, whereas the structure **T6/Pd4_1_c1_(f,f)** contains H-ligands on the Pd−Pd−Pd faces. As seen in Figure 3, the most stable singlet products of Path(1) retain the η^3 Pd−O_1 coordination mode, with the Pd−O_1 distances of 2.69, 3.00 and 3.00 Å for **T6/Pd4_1_c1_(e,e′)**, and 2.71, 2.88 and 2.88 Å for **T6/Pd4_1_c1_(f,f)**.

Let us now discuss the energetics of the reaction **T6/Pd$_4$(1)** + H_2. The calculated $\Delta E_0/\Delta H$ values (relative to the reactants)

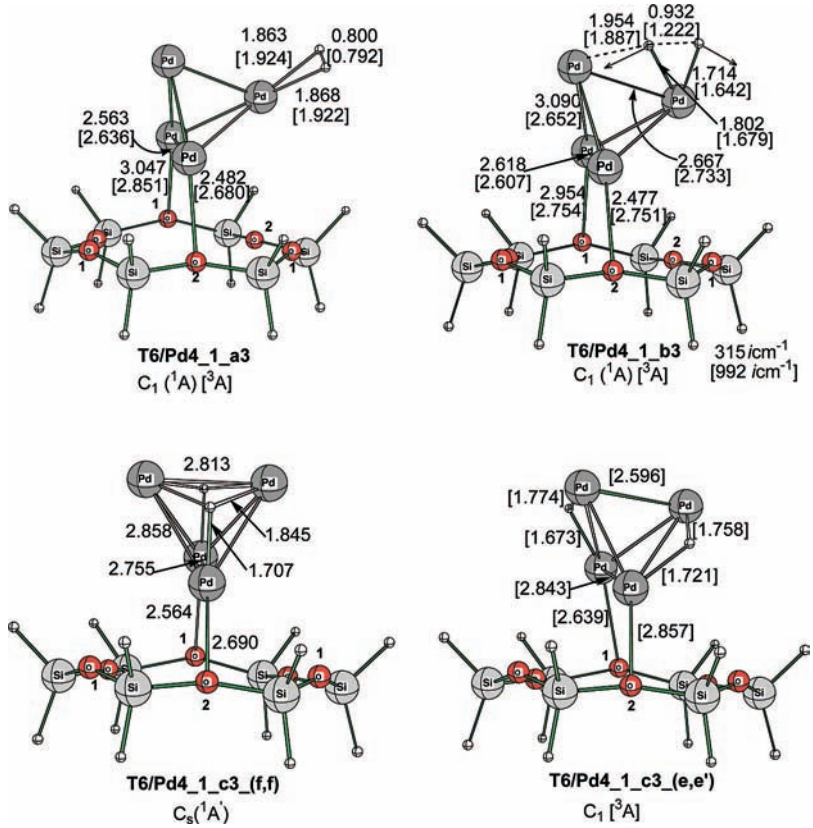

Figure 6. Important geometry parameters (distances in Å, in brackets for triplet) of the intermediates, transition states (with imaginary frequency and reaction coordinate vectors) and products of the singlet and triplet state reaction (Path 3): **T6/Pd$_4$(3)** + H_2.

of the intermediates, transition states and products of reaction **T6/Pd$_4$(1)**(^{3}A″) + H_2 are summarized in Table 2. For comparison, the corresponding results for the unsupported[14b] Pd_4 computed with respect to the Pd_4(^{3}A″) + H_2 dissociation limit are also given in italics in Table 2. For the triplet state prereaction H_2 complex **T6/Pd4_1_a1**(^{3}A″), $\Delta E_0/\Delta H$ values are −5.9/−6.7 kcal/mol, which are slightly smaller (in absolute sense) than the numbers −7.0/−7.7 kcal/mol for the unsupported Pd_4. More importantly, the favored triplet state *basal* TS **T6/Pd4_1_b1**(^{3}A″) lies 3.2/2.0 kcal/mol above the reactants; thus, the barrier for the triplet state T6-supported reaction is lowered by only 0.8/0.8 kcal/mol compared to its gas-phase unsupported analog. By contrast, for the triplet state *apical* TS **T6/Pd4_1_b1′**(^{3}A), the barrier of 4.8/3.7 kcal/mol for the T6-supported system is increased by 0.8/0.9 kcal/mol relative to the unsupported case. For the high-energy singlet state *apical* TS **T6/Pd4_1_b1′** the H−H activation barrier is reduced by 0.7/0.6 kcal/mol but for the *basal* TS **T6/Pd4_1_b1** it is increased by 0.4/0.6 kcal/mol compared to the unsupported Pd_4.

Products of the Path(1), **T6/Pd4_1_c1_(e,e′)** and **T6/Pd4_1_c1_(f,f)**, are computed to be −17.6/−18.9 and −17.0/−18.6 kcal/mol lower in energy than the **T6/Pd$_4$(1)**(^{3}A″) + H_2 reactants, respectively. As seen in Table 2, the hydrogenation of the zeolite-supported Pd_4 along the Path(1) is predicted to be slightly less exothermic, by 1.4/1.4 and 1.3/1.4 kcal/mol, compared to the corresponding unsupported reactions. The calculated triplet state product **T6/Pd4_1_c1_(e,e′)**(^{3}A″) lies higher by 10.8/10.8 kcal/mol than its singlet counterpart.

Path(2). Similarly to the Path(1) case, the hydrogenation of the reference cluster **T6/Pd$_4$(2)**, Path(2), leads initially to the dihydrogen complexes **T6/Pd4_1_a2**(^{1}A′, ^{3}A″) (see Figure 5 and Table 2), whose structures resemble those of **T6/Pd4_1_a1**(^{1}A, ^{3}A″) discussed above and therefore will not be repeated.[33] The following H−H activation occurs through transition states **T6/Pd4_1_b2**(^{1}A′,^{3}A″), which exhibit same gas phase-like structures encountered for the Path(1) TSs (see above). Compared to the gas-phase reaction,[14b] the H_2 molecule starts to dissociate earlier at both the singlet (with the broken H−H distance of 0.916 Å) and triplet (with the broken H−H distance of 1.250 Å) transition states of Path(2). A significant energetic feature of the lower energy triplet state TS **T6/Pd4_1_b2**(^{3}A″) is that it lies only 2.2/0.7 kcal/mol above the **T6/Pd$_4$(2)**(^{3}A″) + H_2 reference, indicating that the T6-support reduces this H−H activation barrier by 1.8/2.1 kcal/mol, relative to the barrier for the unsupported Pd_4 cluster. This is consistent with the relatively strong η^3 binding mode of the Pd_4-fragment to the T6-support at the TS **T6/Pd4_1_b2**(^{3}A″), manifested by the three relatively short Pd−O_2 contacts of 2.57, 2.57 and 2.58 Å. Note that these Pd−O contacts of the triplet η^3 TS of Path(2) are significantly shorter than those of the Path(1) counterpart.

The "direct" singlet state product of Path(2), **T6/Pd4_1_c2_(e,e′)**, which features the conserved η^3 coordination mode with the Pd−O_2 contacts of 2.61, 3.13 and 3.13 Å appeared to be unstable, showing an imaginary frequency of the order of 50i cm^{-1} (this cluster is included in Supporting Information). The subsequent reoptimization of the cluster with the H bridging pattern changed from (**e,e′**) to (**f,f**) resulted in a stable cluster **T6/Pd4_1_c2_(f,f)**, calculated to be 1.5/1.5 kcal/mol lower in energy than **T6/Pd4_1_c2_(e,e′)**. The former hydrogenation product represents a different binding mode of Pd_4 to the zeolite support, compared to the Path(1) analog, with the "upside-down" $Pd_4(H)_2$ unit coordinated to T6 via the single Pd atom. In addition to the retained short Pd−O_2 distance of 2.60 Å in **T6/Pd4_1_c2_(f,f)**, the Pd_4 cluster is also weakly coordinated to two O_1 sites. The calculated $\Delta E_0/\Delta H$ of **T6/Pd4_1_c2_(f,f)** is −19.2/−21.0 kcal/mol with respect to the **T6/**

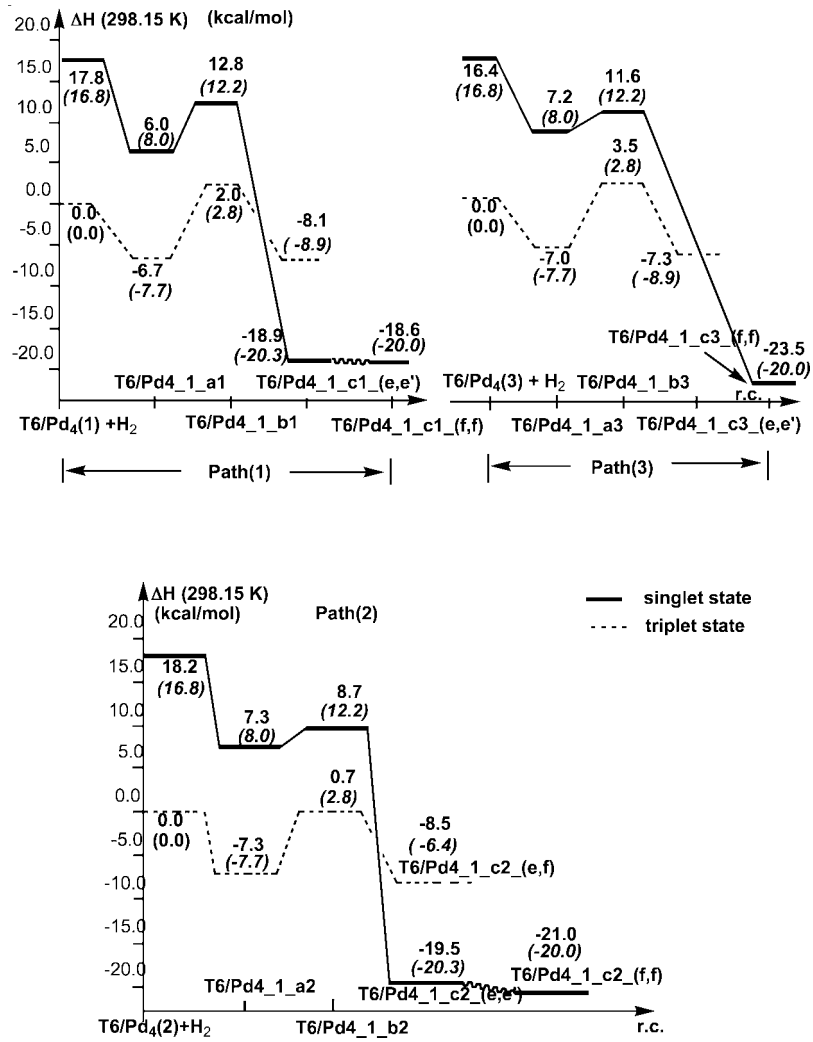

Figure 7. Calculated potential energy profiles of the singlet and triplet state reactions, **T6/Pd$_4$(1)** + H_2 (Path(1)), **T6/Pd$_4$(2)** + H_2 (Path(2)), and **T6/Pd$_4$(3)** + H_2 (Path(3)). For the Path(1), the most favorable *basal* TS energy is provided. The numbers given in parentheses are for the gas phase Pd_4 + H_2 reaction (taken from ref 14b).

Pd$_4$(2) (^{3}A″) + H_2 reference. Consequently, the H_2 activation along the Path(2) is found to be more exothermic by 0.9/1.0 kcal/mol than that for unsupported Pd_4 cluster. The "upside-down" triplet state product, **T6/Pd4_1_c2_(e,f)**(^{3}A) (note the change to the **(e,f)** bridging), is energetically not competitive with the singlet state product.

Path(3). Path(3) starts from the cluster **T6/Pd$_4$(3)**, where Pd_4 has attached to T6 via the Pd−Pd edge. The H_2 coordination to the Pd atom that is not involved in the Pd−O binding results in the formation of the complex **T6/Pd4_1_a3**(^{1}A, ^{3}A) (Figure 6). From this complex, the reaction continues via the H−H activation TS **T6/Pd4_1_b3**(^{1}A, ^{3}A) with the preserved η^2 T6/Pd_4 binding mode. In the singlet state of **T6/Pd4_1_b3**, the breaking H−H distance of 0.932 Å is very close to that for unsupported Pd_4 cluster. In the lower energy triplet state of **T6/Pd4_1_b3**(^{3}A), however, this H−H distance at 1.222 Å is somewhat shorter compared to the unsupported reaction (of 1.266 Å). Similar to the transition states located on the Path(1) and Path(2), the characteristic four-center motive of Pd_4−H_2 is seen for the singlet and triplet state **T6/Pd4_1_b3**(^{1}A, ^{3}A) structures. The lower energy triplet state TS is found to be 4.8/3.5 kcal/mol above the **T6/Pd$_4$(3)**(^{3}A) + H_2 reference, implying that T6-support increases the H−H activation barrier by 0.8/0.7 kcal/mol relative to the gas phase barrier. The support effect on the barrier height for the η^2 TS **T6/Pd4_1_b3**(^{3}A) of Path(3) resembles that of the less favored η^1 *apical* TS **T6/Pd4_1_b1′** (^{3}A) of Path(1).

The most preferred singlet state product of Path(3) is **T6/Pd4_1_c3_(f,f)** structure, which retains the η^2 T6/Pd_4 binding mode, with the relatively short Pd−O_1 and Pd−O_2 bonds of 2.56 and 2.69 Å, respectively. Interestingly, the calculated ΔE_0/ΔH for the reaction **T6/Pd$_4$(3)**(^{3}A) + H_2 → **T6/Pd4_1_c3_(f,f)**, −21.8/−23.5 kcal/mol, indicates more exothermic hydrogenation by 3.5/3.5 kcal/mol compared to the unsupported case. The triplet state cluster **T6/Pd4_1_c3_(e,e′)**(^{3}A) (note the changed H bridging pattern relative to the singlet) lies again much higher in energy.

The singlet and triplet state ΔH profiles of Path(1), Path(2) and Path(3) are shown in Figure 7. Qualitatively, these profiles are similar to those found for the unsupported Pd_4 + H_2 reaction,[14b] especially in terms of the location of triplet-singlet crossing after the H−H bond activation TS. Clearly, the zeolite support causes the appearance of distinct H−H activation routes as well as various binding modes of $Pd_4(H)_2$, but without changing the preferred spin state and structures of the most stable products. For the lower energy triplet state T6-supported TSs, the H−H bond activation barrier (ΔE_0/ΔH) increased in the order Path(2) (2.2/0.7) < Path(1) (3.2/2.0) < Path(3) (4.8/3.5). The exothermicity of the overall reaction of the first H_2 addition was found to increase in the order: Path(1) < Path(2)

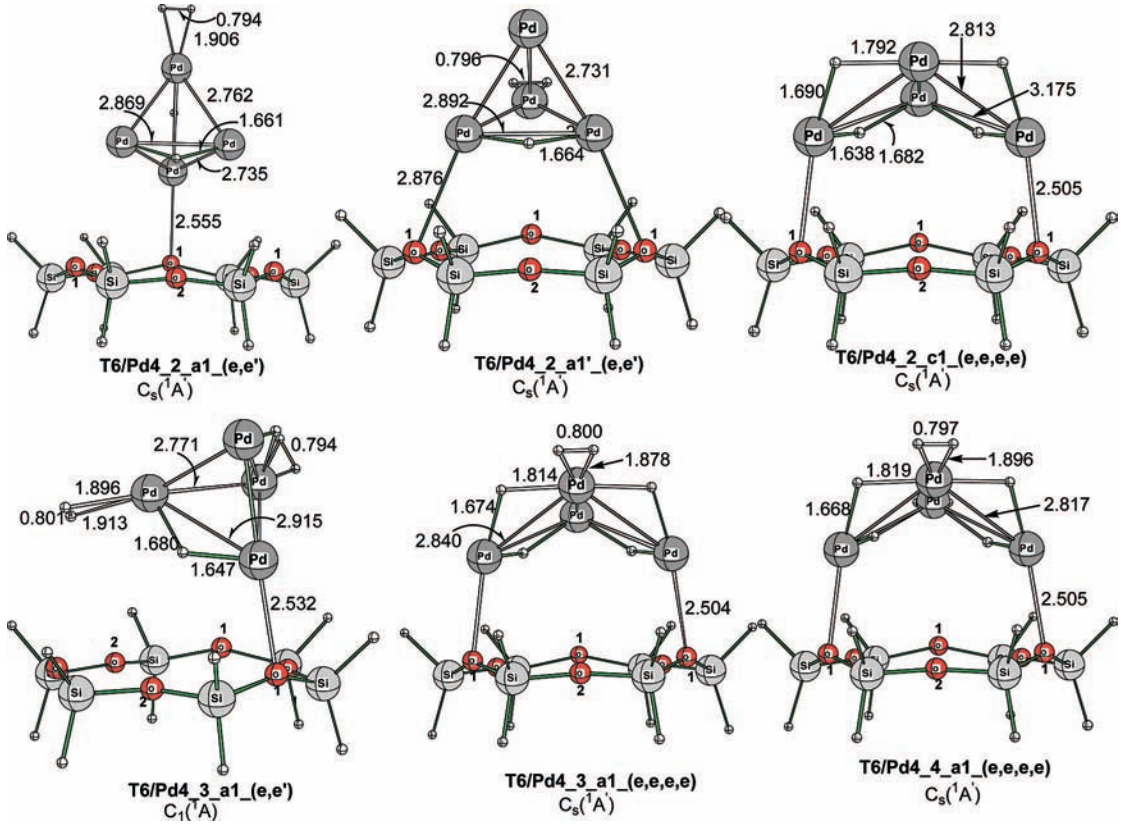

Figure 8. Important geometry parameters (distances in Å) of the H_2 complexes pertinent to the adsorption of the second, third and fourth H_2 molecule on the hydrogenation product of Path(1), **T6/Pd4_1_c1_(e,e′)**.

TABLE 3: Calculated Relative Energies (Relative to the Corresponding Reactants, in kcal/mol) of the Important Intermediates of the Second, Third and Fourth H_2 Molecule Addition to the Products of the First H_2 Addition to T6/Pd_4(1), T6/Pd_4(2) and T6/Pd_4(3)[a]

supported cluster		ΔE		ΔE_0[b]		ΔH[c]	
Path(1) Continued							
T6/$Pd_4(H)_2$ + mH_2	**T6/Pd4_1_c1_(e,e′)** + mH_2	0.0	*0.0*	0.0	*0.0*	0.0	*0.0*
T6/$Pd_4(H)_2(H_2)$	**T6/Pd4_2_a1_(e,e′)**	−10.8	*−10.8*	−9.2	*−9.2*	−9.8	*−9.9*
T6/$Pd_4(H)_2(H_2)$	**T6/Pd4_2_a1′_(e,e′)**	−9.5	*−10.8*	−7.9	*−9.2*	−8.6	*−9.9*
T6/$Pd_4(H)_4$	**T6/Pd4_2_c1_(e,e,e,e)**	−11.2	*d*	−9.4	*d*	−11.2	*d*
T6/$Pd_4(H)_2(H_2)_2$	**T6/Pd4_3_a1_(e,e′)**	−22.6	*−21.0*	−19.1	*−17.7*	−20.7	*−19.1*
T6/$Pd_4(H)_4(H_2)$	**T6/Pd4_3_a1_(e,e,e,e)**	−23.7	*d*	−19.4	*d*	−22.3	*d*
T6/$Pd_4(H)_4(H_2)_2$	**T6/Pd4_4_a1_(e,e,e,e)**	−32.0	*d*	−25.7	*d*	−29.5	*d*
Path(2) Continued							
T6/$Pd_4(H)_2$ + mH_2	**T6/Pd4_1_c2_(f,f)** + mH_2	0.0	*0.0*	0.0	*0.0*	0.0	*0.0*
T6/$Pd_4(H)_2(H_2)$	**T6/Pd4_2_a2_(f,f)**	−12.8	*−10.0*	−10.9	*−8.8*	−11.8	*−9.9*
T6/$Pd_4(H)_2(H_2)_2$	**T6/Pd4_3_a2_(f,f)**	−23.9	*−22.2*	−20.3	*−19.3*	−21.9	*−21.2*
T6/$Pd_4(H)_2(H_2)_3$	**T6/Pd4_4_a2_(f,f)**	−34.5	*e*	−28.9	*e*	−31.2	*e*
Path(3) Continued							
T6/$Pd_4(H)_2$ + mH_2	**T6/Pd4_1_c3_(f,f)** + mH_2	0.0	*0.0*	0.0	*0.0*	0.0	*0.0*
T6/$Pd_4(H)_2(H_2)$	**T6/Pd4_2_a3_(f,f)**	−11.6	*−10.0*	−9.4	*−8.8*	−10.3	*−9.9*
T6/$Pd_4(H)_2(H_2)_2$	**T6/Pd4_3_a3_(f,f)**	−22.2	*−22.2*	−18.1	*−19.3*	−19.7	*−21.2*
T6/$Pd_4(H)_2(H_2)_3$	**T6/Pd4_4_a3_(f,f)**	−30.4	*e*	−24.9	*e*	−27.9	*e*

[a] All states are in singlet and values given in italics are for the gas-phase reaction $Pd_4 + H_2$, taken from the ref 14b. See Figures 3–5 for the definition of the T6/$Pd_4(H)_2$ reference clusters. [b] $\Delta E_0 = \Delta E + \Delta ZPE$, zero-point energy corrections were calculated at the B3LYP/HWDZP level. [c] ΔH, enthalpies were calculated at the 1 atm and 298.15 K at the B3LYP/TZP//B3LYP/HWDZP level. [d] The gas phase cluster is not stable.[14b] [e] The gas phase cluster of this kind was not previously found.[14b]

< Path(3), with the most favorable heat of reaction of −21.8/−23.5 kcal/mol for Path(3).

D. Multiple H_2 Molecules on T6/Pd_4. In this section, we describe the sequential adsorption of more than one H_2 molecule on the zeolite-supported Pd_4 cluster. Here, we use the most stable products of the reactions Path(i), $i = 1-3$ as reactants for the next H_2 additions.

Continuation of Path(1). As expected on the basis of the experience gained from the previous studies of the gas-phase reaction of **Pd4_1_c1_(e,e′)** ($Pd_4(H)_2$) with another H_2 molecule, coordination of H_2 to the *apical* and *basal* Pd atoms of **T6/Pd4_1_c1_(e,e′)** resulted in the H_2 complexes **T6/Pd4_2_a1_(e,e′)** and **T6/Pd4_2_a1′_(e,e′)** with the bishydrido-dihydrogen formula T6/$Pd_4(H)_2H_2$, as shown in Figure 8.

However, due to the zeolite-support, the structure **T6/Pd4_2_c1_(e,e,e,e)** of tetrahydride formula T6/$Pd_4(H)_4$ corresponding to the dissociative addition of the second H_2 molecule to the supported $Pd_4(H)_2$ became the energetically most favorable complex with $\Delta E_0/\Delta H$ of −9.4/−11.2 kcal/mol, more favorable than the complexes **T6/Pd4_2_a1_(e,e′)** and **T6/Pd4_2_a1′_(e,e′)** by 0.2/1.4 and 1.5/2.6 kcal/mol, respectively (Table 3). We call the structure **T6/Pd4_2_c1_(e,e,e,e)** "novel" because the $Pd_4(H)_4$ structure without zeolite support was not stable at the gas-phase studies.[14b] As seen in Figure 8, zeolite support of the $Pd_4(H)_4$ cluster resulted in cleavage of one of the Pd−Pd bonds and considerable elongation of the other Pd−Pd bonds. Apparently, the compensating stabilization of $Pd_4(H)_4$ moiety by the support occurs by the two relatively short Pd−O_1 bonds of 2.51 Å as well as the newly formed three-centered Pd−H−Pd bonds.

Another zeolite-unique structure originates from accommodation of the third H_2, where the tetrahydrido−dihydrogen T6/$Pd_4(H)_4H_2$ structure **T6/Pd4_3_a1_(e,e,e,e)** is found to be more stable by 0.3/1.6 kcal/mol than the bishydrido−bis(dihydrogen) T6/$Pd_4(H)_2(H_2)_2$ complex **T6/Pd4_3_a1_(e,e′)** (Table 3), whereas in the gas phase such a tetrahydride structure has never been found. Similarly, the added fourth H_2 molecule gives rise to the tetrahydrido-dihydrogen T6/$Pd_4(H)_4(H_2)_2$ structure **T6/Pd4_4_a1_(e,e,e,e)** that was never found in the gas phase. Finally, concerning the total number of H_2 molecules bound, on the supported Pd_4 cluster four was the maximum number of H_2 molecules that can be adsorbed as seen in **T6/Pd4_4_a1_(e,e,e,e)**, whereas on the gas phase unsupported Pd_4, five was the maximum in the form of $Pd_4(H)_2(H_2)_4$.[14b] This is obviously due to the involvement of some Pd_4 sites in the interaction with T6.

Continuation of Path(2). The uptake of the second, third and fourth H_2 onto the hydrogenated product of Path(2), **T6/Pd4_1_c2_(f,f)**, gives rise to the H_2 complex clusters **T6/Pd4_2_a2_(f,f)**, **T6/Pd4_3_a2_(f,f)** and **T6/Pd4_4_a2_(f,f)**, respectively (shown in Figure 1S of Supporting Information). These T6/$Pd_4(H)_2(H_2)_n$ ($n = 1-3$) clusters contain only one dissociatively adsorbed H_2 (no dissociative addition product T6/$Pd_4(H)_4$ was found). However, the H_2 additions are found to be more exothermic in the continuation of Path(2) compared to those for continuation of Path(1) and (3), likely due to the more Pd centers available for H_2 addition in **T6/Pd4_1_c2_(f,f)**. Indeed, the "upside down" T6/$Pd_4(H)_2$ structure is preserved in all the complexes, with one short (2.50−2.54 Å) Pd−O_2 and two long (3.20−3.23 Å) Pd−O_1 bonds. It is also worth noting that upon accepting the successive H_2 molecules, the Pd−O_2 distance actually decreases for the ensuing "hydrogen-rich" clusters (cf. Figure 1S of Supporting Information).

Continuation of Path(3). We have also investigated addition of the second, third and fourth H_2 molecule to **T6/Pd4_1_c3_(f,f)**, the Path(3) product of the first H_2 addition to T6-supported Pd_4 cluster. It was found that the sequential H_2 adsorption gives rise again to the dihydrogen complex clusters T6/$Pd_4(H)_2(H_2)_n$ ($n = 1-3$): **T6/Pd4_2_a3_(f,f)**, **T6/Pd4_3_a3_(f,f)** and **T6/Pd4_4_a3_(f,f)**(shown in Figure 2S of Supporting Information). Thus, no dissociative addition products of the second, third and fourth H_2 molecule to **T6/Pd4_1_c3_(f,f)** were found.

In summary, our results clearly show that the addition of the second, third and fourth H_2 molecules to the first H_2 addition products of the Path(i) ($i = 1-3$) leads to the dissociative (oxidative) addition product only for the continuation of Path(1). However, one also should note that the dihydrogen complexes of the continuation of Path(2) are energetically more favorable than both the dihydrogen complexes of the continuation of Path(3) and dihydride complexes of the continuation of Path(1).

IV. Conclusions

From the above presented results/discussion one may draw the following conclusions:

(a) Pd_4 cluster binds to the O-centers of T6 support via three different ways leading to three different structures **T6/Pd_4(*i*)**, $i = 1-3$ involving η^3 and η^2 coordination of Pd_4 to T6. For the energetically most stable triplet state structures, the calculated Pd−O distances are 2.64−2.78 Å and energy of interaction between T6 and Pd_4 is ca. −5 kcal/mol. These findings are consistent with the EXAFS[11a,29b] and recent DFT results.[30]

(b) Encapsulating Pd_4 within the sodalite cage (T24 cluster) followed by the full geometry optimization of the resulted **T24/Pd_4** cluster indicated no significant structure distortion or spin quenching of Pd_4 moiety. The BSSE corrected "zeolite"-Pd_4 interaction energy in **T24/Pd_4** is ca. −7 kcal/mol.

(c) The H−H bond activation barrier ($\Delta E_0/\Delta H$, kcal/mol) associated with the first H_2 addition to **T6/Pd_4(*i*)** clusters, called Path(i), increases in the order: Path(2) (2.2/0.7) < Path(1) (3.2/2.0) < Path(3) (4.8/3.5). Comparison of the H_2 addition barriers between T6-supported and gas-phase[14b] Pd_4 indicates that embedding of Pd_4 on the zeolite reduces this barrier slightly (by 1.8/2.1 kcal/mol) but does not change the characteristic Pd_4-H_2 active site structural motive.

(d) The exothermicity of the first H_2 addition to **T6/Pd_4(i)** increases in the order: Path(1) < Path(2) < Path(3).

(e) Addition of the second, third and fourth H_2 ($n = 1-3$) molecules to the first H_2 addition product of the Path(1) leads to novel dissociative adsorption tetrahydride species that were not found in the gas phase: a T6/$Pd_4(H)_4$ structure **T6/Pd4_2_c1_(e,e,e,e)**, a T6/$Pd_4(H)_4H_2$ structure **T6/Pd4_3_a1_(e,e,e,e)** and a T6/$Pd_4(H)_4(H_2)_2$ structure **T6/Pd4_4_a1_(e,e,e,e)**. However, these tetrahydride complexes are higher in energy than the bishydride complexes formed in the continuation of Path(2).

Acknowledgment. J.M. acknowledges the Emerson Center of Emory University for the Visiting Fellowship. He also thanks the staff of the Emerson Center for kind help and for the use of the computer facilities and programs. J.M. extends further his thanks to Drs. Rozanska, Marie and Hriljac for copies of refs 5, 9 and 10a, respectively. Acknowledgement is also made for generous support of computer time at the Emerson Center.

Supporting Information Available: Full ref 25. Cartesian coordinates of all the structures discussed in the paper. T6/Pd_4 clusters with Pd_4 interacting via the apex. Top views of the T6 supported Pd_4 clusters and supported clusters relevant to molecular and dissociative adsorption of the first H_2 molecule on **T6/Pd_4(1)**, **T6/Pd_4(2)** and **T6/Pd_4(3)**. The H_2 complex **T6/Pd4_1_a1′** resulting from the apical adsorption on **T6/Pd_4**. Dihydrogen complexes pertinent to adsorption of the second, third and fourth H_2 molecule onto the hydrogenation product of Path(2), **T6/Pd4_1_c2_(f,f)** and onto hydrogenation product of Path(3), **T6/Pd4_1_c3_(f,f)**. This material is available free of charge via the Internet at http://pubs.acs.org.

References and Notes

(1) Meier, W. M.; Olson, D. H. *Atlas of Zeolite Structure Types*, 3rd revised ed.; Butterworth-Heinemann: London,1992.

(2) Barrer, R. M. *Zeolite and Clay Minerals as Sorbens and Molecular Sieves*; Academic Press: New York, 1978.

(3) *Handbook of Zeolite Science and Technology*; Auerbach, S. M., Carrado, K. A., Dutta, P. K., Eds.; Marcel Dekker: New York, 2003.

(4) (a) Sachtler, W. M. H. *Acc. Chem. Res.* **1993**, *26*, 383. (b) Okumura, K.; Yoshimoto, R.; Uruga, T.; Tanida, H.; Kato, K.; Yokota, S.; Niwa, M. J. *J. Phys. Chem. B* **2004**, *108*, 6250.

(5) Rozanska, X.; Barbosa, L. A. M. M.; van Santen, R. A. *J. Phys. Chem. B* **2005**, *109*, 2203, and references cited therein.

(6) Chen, N. Y.; Degnan, T. F., Jr.; Smith, C. M. *Molecular Transport and Reaction in Zeolites, Design and Application of Shape Selective Catalyst*; VCH Publishers: New York, 1994.

(7) Thomas, J. M.; Thomas, W. J. *Principles and Practice of Heterogeneous Catalysis*; VCH Publishers: Weinheim, 1997.

(8) Baerlocher, C. ; Meier, W. M. ; Olson, D. H. *Atlas of Zeolite Framework*; Elsevier: Amsterdam, 2001.

(9) Sarria, F. R.; Marie, O.; Saussey, J.; Daturi, M. *J. Phys. Chem. B* **2005**, *109*, 1660.

(10) (a) Hriljac, J. A.; Eddy, M. M.; Cheetham, A. K.; Donohue, J. A.; Ray, G. J. *J. Solid State Chem.* **1993**, *106*, 66. (b) Colligan, M.; Forster, P. M.; Cheetham, A. K.; Lee, Y.; Vogt, T.; Hriljac, J. A. *J. Am. Chem. Soc.* **2004**, *126*, 12015. (c) Henson, N. J.; Cheetham, A. K.; Stockenhuber, M.; Lercher, J. A. *J. Chem. Soc., Faraday Trans.* **1998**, *94*, 3759.

(11) (a) Moller, K.; Koningsberger, D. C.; Bein, T. *J. Phys. Chem.* **1989**, *93*, 6116. (b) Moller, K.; Bein, T. *J. Phys. Chem.* **1990**, *94*, 845. (c) Zhang, Z.; Chen, H.; Sheu, L.-L. *J. Catal.* **1991**, *127*, 213. (d) Bai, X.; Sachtler, W. M. H. *J. Catal.* **1991**, *129*, 121. (e) Zhang, Z.; Chen, H.; Sachtler, W. M. H. *J.Chem.Soc.Faraday Trans.* **1991**, *87*, 1413. (f) Kim, J. G.; Ihm, S. K.; Lee, J. Y.; Ryoo, R. *J. Phys. Chem.* **1991**, *95*, 8546. (g) Zhang, Z.; Sachtler, W. M. H. *J. Mol. Catal.* **1991**, *67*, 349. (h) Ryoo, R.; Cho, S. J.; Pak, C.; Kim, J. G.; Ihm, S. K.; Lee, J. Y. *J. Am. Chem. Soc.* **1992**, *114*, 76. (i) Stakheev, A.Yu.; Sachtler, W. M. H. *J. Chem. Soc., Faraday Trans.* **1991**, *87*, 3703. (j) Bein, T. *ACS Symposium Series* **1992**, *499*, 274. (k) Beutel, T.; Zhang, Z.; Sachtler, W. M. H.; Knoezinger, H. *J. Phys. Chem.* **1993**, *97*, 3579. (l) Vogel, W.; Sachtler, W. M. H.; Zhang, Z. *Ber. Bunsen-Ges.* **1993**, *97*, 280. (m) Moretti, G. *Zeolites* **1994**, *14*, 469. (n) Sordelli, L.; Martra, G.; Psaro, R.; Dossi, C.; Colluccia, S. *J. Chem. Soc., Dalton Trans.: Inorg. Chem.* **1996**, *5*, 765. (o) Vogel, W.; Knoezinger, H.; Carvill, B. T.; Sachtler, W. M. H.; Zhang, Z. C. *J. Phys. Chem. B* **1998**, *102*, 1750. (p) Novakova, J. *Collect. Czech. Chem. Commun.* **1998**, *63*, 1839.

(12) (a) Nishimiya, N.; Kishi, T.; Mizushima, T.; Matsumoto, A.; Tsutsumi, K. *J. Alloys Compd.* **2001**, *319*, 312. (b) Jiang, Y.-X.; Weng, W.-Z. Si, D.; Sun, S.-G. *J. Phys. Chem. B* **2005**, *109*, 7637.

(13) Yokoyama, T.; Kimoto, S.; Ohta, T. *Physica B* **1989**, *158*, 255.

(14) (a) Cui, Q.; Musaev, D. G.; Morokuma, K. *J. Phys. Chem. A* **1998**, *102*, 6373. (b) Moc, J.; Musaev, D. G.; Morokuma, K. *J. Phys.Chem. A* **2000**, *104*, 11606. (c) Moc, J.; Musaev, D. G.; Morokuma, K. *J. Phys. Chem. A* **2003**, *107*, 4929.

(15) (a) Fitch, A. N.; Jobic, H.; Renouprez, H. *J. Phys. Chem.* **1986**, *90*, 1311. (b) Olson, D. H. *Zeolites* **1995**, *15*, 439. (c) Eulenberger, G. R.; Shoemaker, D. P.; Keil, J. G. *J. Phys. Chem.* **1967**, *71*, 1812.

(16) (a) Sauer, J.; Sierka, M. *J. Comput. Chem.* **2000**, *21*, 1470. (b) Sauer, J. In *Modelling of Structure and Reactivity in Zeolites*; Catlow, C. R. A., Ed.; Academic Press: London, 1992. (c) Sauer, J. *Chem. Rev.* **1989**, *89*, 199. (d) Sauer, J.; Ugliengo, P.; Garrone, E.; Saunders, V. R. *Chem. Rev.* **1994**, *94*, 2095.

(17) Ferrari, A. M.; Neyman, K. M.; Mayer, M.; Staufer, M.; Gates, B. C.; Rösch, N. *J. Phys. Chem. B* **1999**, *103*, 5311.

(18) (a) Becke, A. D. *Phys. Rev. A* **1988**, *38*, 3098. (b) Lee, C.; Yang, W.; Parr, R. G. *Phys. Rev. B* **1988**, *37*, 785.

(19) (a) Hay, P. J.; Wadt, W. R. *J. Chem. Phys.* **1985**, *82*, 270. (b) Hay, P. J.; Wadt, W. R. *J. Chem. Phys.* **1985**, *82*, 284. (c) Hay, P. J.; Wadt, W. R. *J. Chem. Phys.* **1985**, *82*, 299.

(20) Dunning, T. H., Jr. *J. Chem. Phys.* **1970**, *53*, 2823. For Pd and H, this basis set is the same as BSI used in our previous study on the $Pd_4 + nH_2$ reactions.[14b]

(21) Jung, Y.; Akinaga, Y.; Jordan, K. D.; Gordon, M. S. *Theor. Chem. Acc.* **2003**, *109*, 268.

(22) Møller, C.; Plesset, M. S. *Phys. Rev.* **1934**, *46*, 618.

(23) (a) Krishnan, R.; Binkley, J. S.; Seeger, R.; Pople, J. A. *J. Chem. Phys.* **1980**, *72*, 650. (b) Frisch, M. J.; Pople, J. A.; Binkley, J. S. *J. Chem. Phys.* **1984**, *80*, 3265.

(24) (a) Andrae, D.; Haussermann, U.; Dolg, M.; Stoll, H.; Preuss, H. *Theor.Chim.Acta* **1990**, *77*, 123. (b) Dunning, T. H., Jr. *J. Chem. Phys.* **1989**, *90*, 1007 As in our previous study (see Ref. 14b), the d functions on H were excluded from this aug-cc-pVTZ basis set. Spin-restricted and spin-unrestricted calculations were performed for the closed- and open-shell systems, respectively.

(25) Frisch, M. J. et al. *Gaussian 03*, revision B.05; Gaussian, Inc.: Pittsburgh, PA, 2003.

(26) Gomes, J. R. B.; Lodziana, Z.; Illas, F. *J. Phys. Chem. B* **2003**, *107*, 6411.

(27) Except for the singlet state cluster **T6/Pd$_4$(2)** which shows an imaginary frequency of 208i cm^{-1} (a″).

(28) TheT6/Pd_4 cluster at its the most stable triplet state features three Pd−O contacts of 3.08Åand produces small imaginary frequency.

(29) (a) The sum of the atomic radii of Pd and O is 2.1Å. *CRC Handbook of Chemistry and Physics*, 74th ed.; CRC Press: Boca Raton, FL, 1993. (b) Unfortunately, EXAFS structural data for Pd_4 clusters in the purely siliceous FAU zeolite, which would be most relevant to the zeolite model employed in the calculations, are not available. The NaX FAU zeolite data were therefore used instead. However, as noticed by the reviewer, the experiment (ref 11a) concerning NaX zeolite gives 1.5 Pd and 2.1 O neighbors for each Pd atom, whereas the computed structure corresponds to 3 Pd and 1 O neighbors. The two FAU zeolite environments are thus not strictly comparable.

(30) Vayssilov, G. N.; Rösch, N. *Phys. Chem. Chem. Phys.* **2005**, *7*, 4019.

(31) Reed, A. E.; Curtiss, L. A.; Weinhold, F. *Chem. Rev.* **1988**, *88*, 899.

(32) Boys, S. F.; Bernardi, F. *Mol. Phys.* **1970**, *19*, 553.

(33) Only the *basal* TS has been investigated for Path(2) because the TS of this type has been found to be more favorable than the *apical* TS (triplet) for Path(1).

JP711403X